Received: 1 October 2020 | Accepted: 13 October 2020 | Published online: 19 November 2020

DOI: 10.1002/dad2.12133

Alzheimer's & Dementia
Diagnosis, Assessment & Disease Monitoring

RESEARCH ARTICLE

Evaluation of a visual interpretation method for tau-PET with ^{18}F-flortaucipir

Ida Sonni[1,2] | **Orit H. Lesman Segev**[3,4] | **Suzanne L. Baker**[1] | **Leonardo Iaccarino**[3] | **Deniz Korman**[5] | **Gil D. Rabinovici**[1,3,6] | **William J. Jagust**[1,5] | **Susan M. Landau**[5] | **Renaud La Joie**[3] | **for the Alzheimer's Disease Neuroimaging Initiative***

[1] Molecular Biophysics and Integrated Bioimaging, Lawrence Berkeley National Lab, Berkeley, California, USA

[2] Ahmanson Translational Theranostics Division, Department of Molecular and Medical Pharmacology, University of California, Los Angeles, Los Angeles, California, USA

[3] Memory and Aging Center, University of California, San Francisco, San Francisco, California, USA

[4] Department of Diagnostic Imaging, Sheba Medical Center, Tel Hashomer, Ramat Gan, Israel

[5] Helen Wills Neuroscience Institute, University of California, Berkeley, Berkeley, California, USA

[6] Department of Radiology and Biomedical Imaging, University of California, San Francisco, San Francisco, California, USA

Correspondence
Ida Sonni, Ahmanson Translational Theranostics Division, Department of Molecular and Medical Pharmacology, David Geffen School of Medicine, University of California, Los Angeles, Los Angeles, CA, USA.
E-mail: isonni@mednet.ucla.edu

*Data used in preparation of this article were obtained from the Alzheimer's Disease Neuroimaging Initiative (ADNI) database (adni.loni.usc.edu). As such, the investigators within the ADNI contributed to the design and implementation of ADNI and/or provided data but did not participate in analysis or writing of this report. A complete listing of ADNI investigators can be found at: http://adni.loni.usc.edu/wp-content/uploads/how_to_apply/ADNI_Acknowledgement_List.pdf

Abstract

Introduction: Positron emission tomography targeting tau (tau-PET) is a promising diagnostic tool for the identification of Alzheimer's disease (AD). Currently available data rely on quantitative measures, and a visual interpretation method, critical for clinical translation, is needed.

Methods: We developed a visual interpretation method for ^{18}F-flortaucipir tau-PET and tested it on 274 individuals (cognitively normal controls, patients with mild cognitive impairment [MCI], AD dementia, and non-AD diagnoses). Two readers interpreted ^{18}F-flortaucipir PET using two complementary indices: a global visual score and a visual distribution pattern.

Results: Global visual scores were reliable, correlated with global cortical ^{18}F-flortaucipir standardized uptake value ratio (SUVR) and were associated with clinical diagnosis and amyloid status. The AD-like ^{18}F-flortaucipir pattern had good sensitivity and specificity to identify amyloid-positive patients with AD dementia or MCI.

Discussion: This ^{18}F-flortaucipir visual rating scheme is associated with SUVR quantification, clinical diagnosis, and amyloid status, and constitutes a promising approach to tau measurement in clinical settings.

KEYWORDS
Alzheimer's disease, flortaucipir, qualitative assessment, tau positron emission tomography, visual assessment

1 | BACKGROUND

Positron emission tomography (PET) has transformed the way we study cognitive decline and dementia, offering the possibility to visualize age-associated pathophysiological changes,[1] with major consequences for diagnosis, disease monitoring, and screening strategies for clinical trials. The importance of biomarkers of amyloid beta (Aβ) deposition has been recognized by the National Institute on Aging and the Alzheimer Association (NIA-AA) in 2011.[2] The advancement of Aβ-PET with ^{11}C-Pittsburgh compound B (PiB),[3] and subsequent fluorinated counterparts[4–6] was rapid. Aβ-PET radiotracers are now clinically available and interpreted visually using a binary (positive/negative) read.[4,7] The successful experience of Aβ-PET has prompted the development of PET radiopharmaceuticals targeting the other aggregated protein implicated in Alzheimer's disease (AD) and other neurodegenerative diseases: tau.

Multiple tau-targeted radiopharmaceuticals are being evaluated in humans.[8] The most widely used tracer, ^{18}F-flortaucipir (FTP; previously ^{18}F-T807 and ^{18}F-AV1451),[9–11] binds with high affinity to paired helical filament tau.[12] FTP-SUVR (standardized uptake value ratio) values correlate with cognitive deficits,[13] phosphorylated tau in CSF[14,15] and plasma,[16] and *post mortem* tau burden in neuropathologically proven AD cases.[17,18] FTP signal strongly correlates with neurodegeneration[19–21] and discriminates AD patients from healthy controls and patients with other neurodegenerative diseases with high accuracy.[22,23] Altogether, FTP-PET could be a promising diagnostic tool, although most published work relies on SUVR quantification and a visual interpretation method, critical for clinical translation, is needed.

Several features of FTP-PET complicate the definition of a simple binary read similar to Aβ-PET: strong between-patient variations in signal intensity and regional distribution, mild-to-moderate signal in non-AD associated conditions, and the presence of "off-target" binding. Given these challenges, our goals were: (1) to develop a reliable approach to guide visual interpretation and reporting of FTP-PET scans, (2) to evaluate the ability of FTP-PET visual reads to distinguish Aβ-positive patients with AD dementia (ADdem) and mild cognitive impairment (MCI) from other participants, (3) to compare visual reads to a previously developed definition of tau-positivity using temporal SUVRs.[22]

RESEARCH IN CONTEXT

1. **Systematic review**: Brain imaging has become increasingly important in characterizing patients with cognitive decline in the context of research studies, clinical diagnosis, and clinical trials. Positron emission tomography (PET) radiotracers targeting tau pathology were recently developed and are currently limited to investigational settings. After reviewing the growing literature on flortaucipir-PET, we identified tau-PET as a promising diagnostic tool although a visual interpretation method, critical for clinical translation, is needed.
2. **Interpretation**: Our proposed flortaucipir-PET visual read approach provides ratings that are strongly associated with standardized uptake value ratio quantification, clinical diagnosis, and amyloid beta status across two cohorts with distinct characteristics. Inter- and intrarater reliability for our main indices are strong, suggesting that our visual approach is reproducible and can represent a promising alternative to quantitative tau-PET measurements in clinical settings.
3. **Future directions**: Future investigations including an autopsy-based gold standard are needed to evaluate the exact potential and limitations of tau-PET and the proposed visual approach.

2 | MATERIALS AND METHODS

2.1 | Study design

2.1.1 | Development phase

A pilot phase was first led by a nuclear medicine physician (IS) and a radiologist (OLS) to develop a visual rating scheme, using a set of 60 FTP-PET scans. This phase allowed the readers to (1) gain familiarity with the different FTP patterns across clinical diagnoses, (2) choose a color scale to analyze images, and (3) develop and test a visual read procedure before proceeding to a larger scale analysis. Subjects were selected from the Berkeley Aging Cohort Study/University of California San Francisco (BACS/UCSF) cohort and included 20 cognitively normal controls, 20 patients with a clinical diagnosis of MCI or probable AD dementia, and 20 patients with non-AD neurodegenerative syndromes. This phase was conducted using FTP SUVR images, intensity normalized by mean inferior cerebellar cortex signal.[24]

2.1.2 | Testing phase

The study was conducted on a separate set of 274 non-intensity-normalized, unitless FTP-PET images to make the visual interpretation independent from image processing, which is not often used in clinical settings. Two co-authors (RLJ and SML) selected 274 subjects from two independent cohorts (137 from BACS/UCSF, 137 from Alzheimer's Disease Neuroimaging Initiative [ADNI]), including various clinical syndromes, Aβ-positive and negative cases. Two PET readers (IS and OLS) were unaware of the sample composition. Scans were anonymized, randomized, and independently rated by both readers blinded to clinical diagnosis and any other clinical, radiological, or demographic information using the visual rating method described below. Ten percent of the

TABLE 1 Cohort characteristics

	BACS/UCSF					ADNI		
	YC	OC	MCI	ADdem	non-AD[a]	OC	MCI	ADdem
N	11	51	8	36	31	60	47	30
Age	39.2 ± 16.0	76.8 ± 6.1	71.0 ± 6.0	62.6 ± 8.0	66.6 ± 7.6	75.5 ± 7.0	76.8 ± 7.6	78.5 ± 9.7
Age (range)	21–59	60–93	63–80	48–82	46–79	59–94	60–92	56-94
Females (%)	10 (91%)	24 (46%)	3 (38%)	23 (64%)	15 (48%)	29 (48%)	31 (66%)	14 (47%)
Years of education	16.8 ± 2.0	16.7 ± 1.9	18.3 ± 3.2	16.9 ± 3.0	16.4 ± 3.1	16.5 ± 2.3	16.6 ± 2.9	15.1 ± 2.6
MMSE	29.0 ± 1.5	28.8 ± 1.2	27.9 ± 2.2	21.3 ± 5.0	24.1 ± 5.7	29.1 ± 1.1	28.0 ± 2.0	21.7 ± 4.9
Aβ-positive (%)[b]	0 (0%)[b]	23 (45%)	8 (100%)	36 (100%)	7 (23%)[b]	16 (27%)	20 (43%)	27 (90%)
APOE ε4 carriers (%)[c]	4 (44%)[b]	15 (29%)	5 (63%)	21 (58%)	8 (26%)	19 (32%)	14 (30%)	13 (43%)

Abbreviations: Aβ, amyloid beta; ADdem, patients with a clinical diagnosis of Alzheimer's disease dementia; ADNI, Alzheimer's Disease Neuroimaging Initiative; APOE, apolipoprotein E; BACS, Berkeley Aging Cohort Study; MCI, patients with a clinical diagnosis of mild cognitive impairment; MMSE, Mini-Mental State Examination; non-AD, patients with a clinical diagnosis of non-AD neurodegenerative syndrome; OC, older controls; PET, positron emission tomography; PiB, Pittsburgh compound B; UCSF, University of California San Francisco; YC, young controls.
Notes: Clinical diagnoses were independent from Aβ status. For continuous variables, mean ± SD is indicated unless specified otherwise.
[a]Non AD cases: eight with behavioral variant frontotemporal dementia, seven with non-fluent primary progressive aphasia, six with corticobasal syndrome, four with Parkinson's disease, three with progressive supranuclear palsy, two with semantic variant primary progressive aphasia.
[b]Missing data in the BACS/UCSF data: Aβ status for 7 YC and 1 non-AD (patient with behavioral variant frontotemporal dementia who carried a V337M MAPT mutation known to cause Alzheimer's like 3R/4R paired helical filaments tau), and APOE genotype for 2 YC. The Aβ tracer used in BACS/UCSF was PiB, while in ADNI florbetapir was used for 128 subjects and florbetaben for 9. PiB-PET was missing for a UCSF patient with clinical AD dementia who died 36 months after FTP-PET and showed high Aβ burden at autopsy (Thal 5 and CERAD frequent); this patient was considered Aβ-positive in all tables, figures, and analyses.
[c]APOE ε4 indicates the percentage of patients with APOE ε4/ε2, APOE ε4/ε3 or APOE ε4/ε4.

scans (15 from BACS/UCSF, 15 from ADNI) were randomly selected, assigned a second anonymized number, and read twice to evaluate intra-reader reliability.

2.2 | Study participants

The institutional review boards of all participating institutions approved the study and informed consent was obtained from all participants or authorized representatives. Cohort characteristics are summarized in Table 1.

2.2.1 | Sample 1—BACS/UCSF

Participants were selected from BACS,[25] and the UCSF Memory and Aging Center research cohorts. The sample included cognitively normal individuals, patients with clinical diagnosis of MCI, AD dementia, or non-Alzheimer's neurodegenerative syndromes. Cognitively normal participants included 11 young controls (YC, aged 20 to 60 years) and 55 older controls (OC, age>60).

2.2.2 | Sample 2—ADNI

ADNI is a multi-site longitudinal study.[26] Subjects selected from this cohort included OC and patients with amnestic MCI and probable AD dementia.

2.3 | Magnetic resonance imaging

T1-weighted magnetic resonance imaging (MRI) was used to define the regions of interest (ROI) used for FTP quantification and were not available to the readers. All scans were processed with FreeSurfer 5.3 (http://surfer.nmr.mgh.harvard.edu/) to derive ROIs in each subject's native space (see below).

2.4 | PET acquisition and processing

Details of the PET acquisition are provided in the supporting information.

Briefly, the FTP-PET data were acquired as four 5-minute frames between 80 and 100 minutes after the injection of ≈370 MBq of radiotracer. Frames were realigned and averaged; resulting images were used for the visual read to make the visual interpretation entirely qualitative.

For quantification purposes, SUVR images were created using the inferior cerebellar cortex as the reference region.[24] FreeSurfer segmentation was used to extract the average SUVR value in two ROIs: (1) the entire cortex and (2) a temporal meta-ROI (including bilateral amygdala, entorhinal, parahippocampal, fusiform, and inferior and middle temporal cortices).[22] We used the latter as a quantification-based criteria to define tau-positivity, using the 1.27 threshold derived from independent samples in Ossenkoppele et al.[22]

Aβ-PET was obtained using PiB-PET (135 BACS/UCSF participants), ^{18}F-florbetapir (n = 128, ADNI), or ^{18}F-florbetaben (n = 9, ADNI).

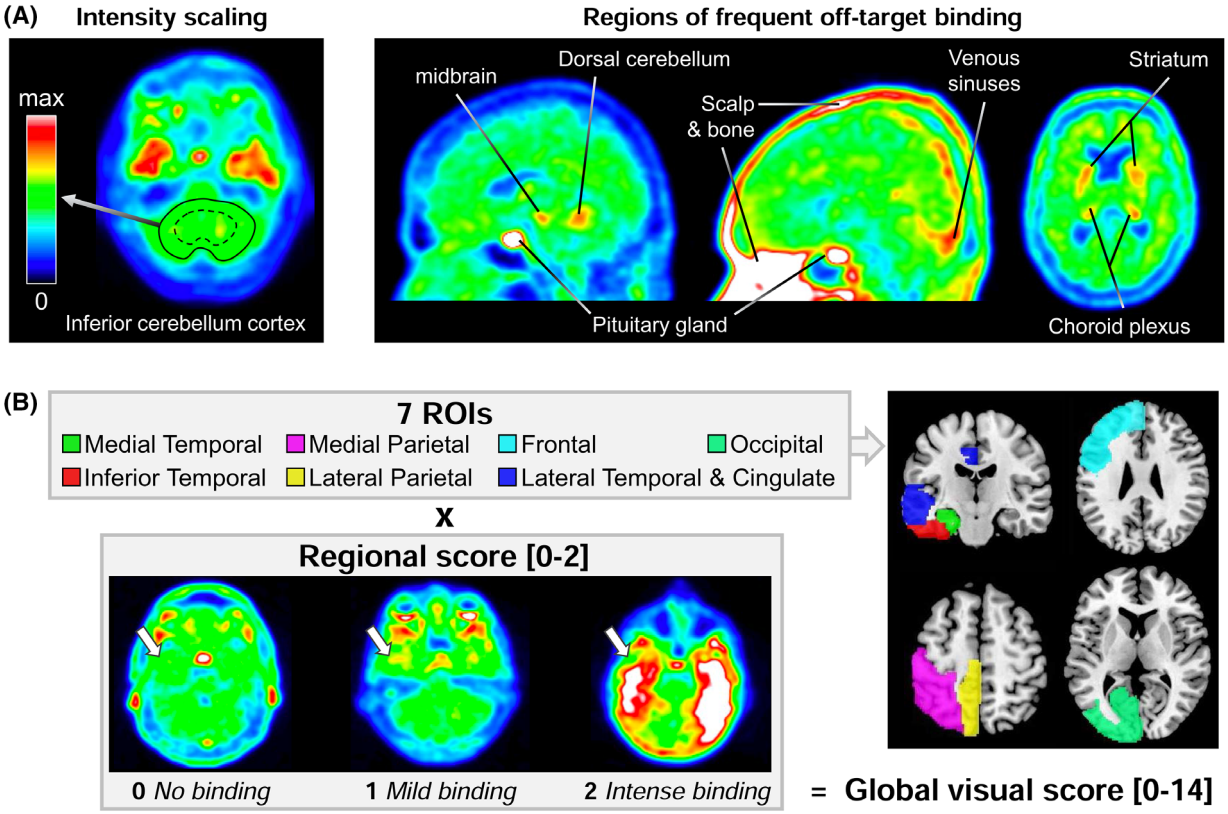

FIGURE 1 Overview of the visual read approach and global score. A, The image intensity has to be manually adjusted by each reader, fixing the value of the inferior cerebellar cortex value to the mid-range of the color scale (green area). For both visual indices (global visual score and flortaucipir pattern), readers considered tracer binding beyond the common areas of off-target (non-specific) binding, as illustrated here in amyloid-negative controls. B, The global visual score is based on seven regions of interest (ROIs), only shown on the left to simplify the display, each scored on a 0 to 2 scale (white arrows illustrate the scale applied to the inferior temporal lobe), resulting in a 0 to 14 global scale

Aβ-PET were processed as previously described and Aβ status was defined from tracer/pipeline specific thresholds: 1.065 DVR for PiB, 1.11 for ^{18}F-florbetapir, and 1.08 for ^{18}F-florbetaben).[19,27–31]

2.5 | FTP-PET visual interpretation method: visual score and distribution pattern

Readers assessed FTP-PET scans with no access to anatomical imaging, using the image viewer software Mango (version 4.0.1–Research Imaging Institute, UTHSCSA; http://ric.uthscsa.edu/mango) and the "Spectrum" color scale. The color scale was manually adjusted so that the predominant color in the inferior cerebellar cortex would be set as the midpoint of the color scale (Figure 1A). Areas of frequent off-target FTP binding[24] (Figure 1A) were taken into consideration. The visual interpretation method provides a report for each FTP scan describing two parameters detailed below.

2.5.1 | Global visual score

FTP-PET images were assessed following a predefined regional cortical binding system (0 = no binding; 1 = mild binding; 2 = intense binding) for seven brain regions (Figure 1B). In the case of asymmetrical uptake within the ROI, that is, higher on one side than on the contralateral, the highest signal intensity was chosen. The global visual score was obtained by summing each score given to the seven cortical ROIs to provide a measure of whole cortex FTP intensity (ranging from 0, no uptake in any of the ROIs, to 14, intense uptake in all ROIs).

2.5.2 | Distribution pattern

Four FTP distribution patterns were described (Figure 2):

- Pattern I (negative scan): absence of FTP signal in any brain area beyond background or off-target binding.
- Pattern II (mild temporal binding only): mild to moderate elevation of FTP signal limited to the medial temporal cortex and fusiform gyrus. This pattern could be consistent with early (ie, I to III) Braak stage tau pathology that can be seen in older individuals with or without cognitive deficits.[32–35]
- Pattern III (AD-like binding): FTP distribution consistent with the neuropathological distribution of tau in Braak stage ≥ IV,[32–35] extending beyond the medial temporal/fusiform area (eg, with lateral temporal, parietal, or frontal cortex binding).

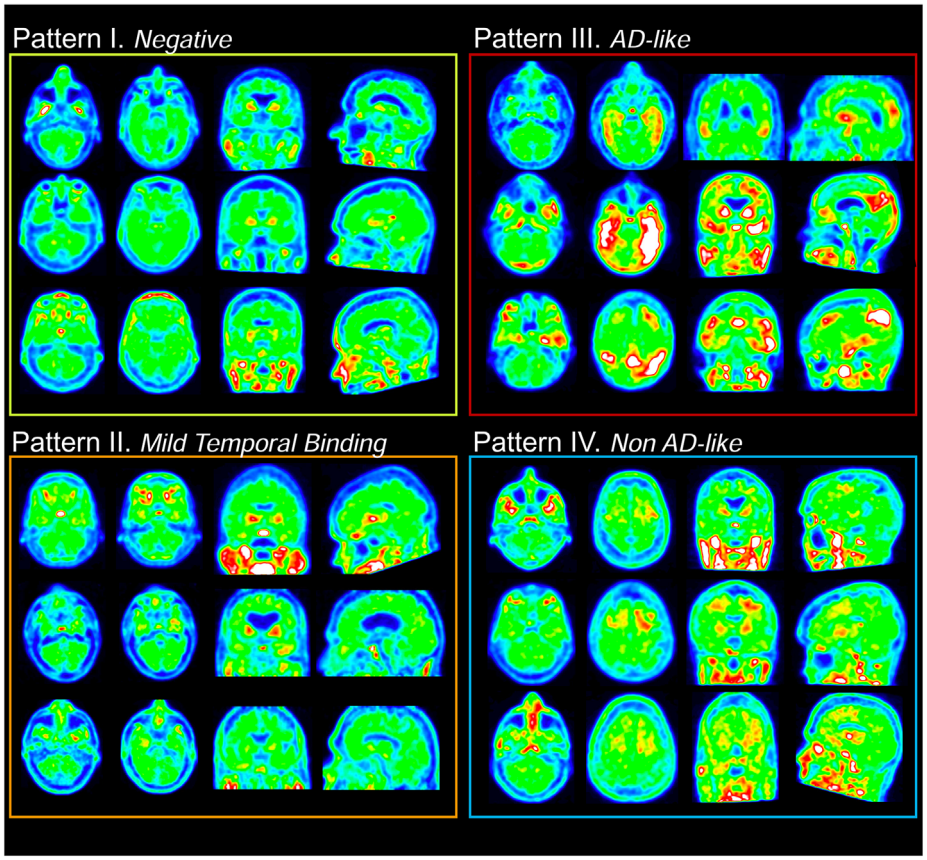

FIGURE 2 Four distribution patterns. Three cases are provided to illustrate each pattern; for all 12 examples shown here, both readers independently assigned the same flortaucipir visual pattern. For each case, four slices are provided, including an axial slice at the level of the inferior cerebellum, and axial, coronal, and sagittal sections throughout the brain

- Pattern IV (non-AD-like): atypical FTP signal distribution, not following the known distribution of tau tangles in AD by Braak et al.[32–35] This pattern includes, but is not limited to, predominant white matter or subcortical binding as previously described in non-AD syndromes.[36]

2.6 | Statistical analysis

Correlations were quantified using Spearman's rho coefficient. The effects of Aβ status and clinical diagnostic on the global visual score was assessed in a general linear model including a group x Aβ interaction term. Relationships between FTP distribution patterns and temporal meta-ROI SUVR or global visual scores were tested using Kruskall Wallis analysis of variance, followed by post hoc pairwise Dwass-Steel-Critchlow-Fligner tests.

Linear weighted kappa (κ) coefficients were used to evaluate inter-rater and intra-rater agreement on the global visual scores; non-weighted κ to evaluate inter- and intra-rater reliability for the identification of the four distribution patterns. When analyzing mismatches between distribution patterns, we distinguished major disagreements (between "negative" and "AD-like" or "AD-like" and "non-AD-like" patterns) from minor disagreements (other combinations). Additional reliability analyses were conducted to specifically focus on reliability of the "AD-like" pattern, versus any of the other patterns.

3 | RESULTS

3.1 | Visual scores: reliability and association with cortical SUVR

Global visual scores from the two readers were strongly correlated (rho = .805, P <.001) and inter-rater agreement was good (linear weighted κ = .73, 95% confidence interval [CI; .68 to .78]; Figure S1A in supporting information). Intra-rater agreement was high: linear weighted $\kappa_{reader1} = 0.79$ [.68 to .91] and $\kappa_{reader2} = 0.84$ [.7 to .93] (Figure S1B).

The average visual score was significantly associated with cortical FTP$^-$SUVR (rho = .71, P <.001; Figure 3A). Inspection of the scatter plot showed a non-linear relationship and differences in dynamic range between the two variables: SUVR values appear little related to the visual score in the low range, while the visual score reaches a ceiling for cortical SUVR >1.6. Complementary analyses were run in three non-overlapping subgroups of similar visual score span, showing that the correlation between SUVR and visual score was significant in low

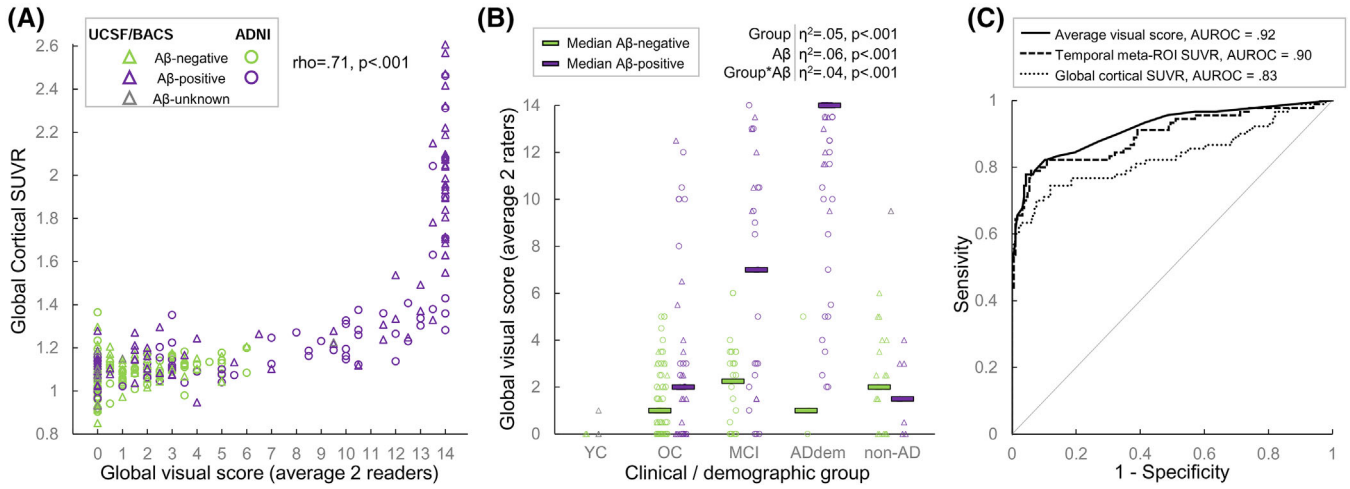

FIGURE 3 Global visual score: association with global cortical standardized uptake value ratio (SUVR), clinical diagnosis, and amyloid status. A, Associations between flortaucipir cortical SUVR and global visual score (average of both readers). See Figure S2 in supporting information for similar plots using each reader's score or each cohort separately. The scatter plot shows a non-linear relationship and differences in dynamic range between the two variables: SUVR values appear little related to the visual score in the low range, while the visual score reaches a ceiling for cortical SUVR >1.6. B, Association of clinical diagnosis and amyloid status on the global visual score (average of both readers). See Figure S3 in supporting information for similar plots using each reader's score. The YC group was excluded from the general linear model results described on top (overall R2 = .68). YC, young controls; OC, older controls; MCI, patients with a clinical diagnosis of mild cognitive impairment; ADdem, patients with a clinical diagnosis of Alzheimer's disease dementia; non-AD, patients with a clinical diagnosis of non-AD neurodegenerative syndrome. Clinical diagnoses were independent from amyloid beta (Aβ) status. C, Receiver operating curve (ROC) testing on the ability of the average global visual score and two SUVR measures to distinguish Aβ-positive MCI/ADdem (n = 90) versus all other participants (n = 184). AUROC, area under the receiver operating curve

values (rho = .29, P <.001 when restricted to scans with a score ≤4), but gradually strengthened with increasing visual scores (rho = .60, for scores between 5 and 9, inclusive; rho = .78 for scores ≥10).

Associations were comparable in strength and shape when looking at each reader's or cohort separately (Figure S2 in supporting information).

3.2 | Visual scores across diagnoses and Aβ status

All but one YC had an average visual score of 0; this group was not included in the following analyses (Figure 3B). In the rest of the cohort, clinical group, Aβ status, and their interaction accounted for 68% of the variance in visual scores. All clinical groups differed from each other (all Ps <.02 using Holm Bonferroni correction), except for the OC and the non-AD group (P = .65). Within Aβ-negative participants, no clinical group difference was significant (all Ps >.5), whereas differences existed between clinical subgroups in Aβ-positive cases (ADdem> MCI > OC and non-AD). Within the OC, MCI, and ADdem clinical groups, visual scores were higher in Aβ-positive patients compared to their Aβ-negative counterparts (P = .023, P <.001 and P <.001, respectively). Receiver operating curve (ROC) analyses were run to assess the ability of the visual score to distinguish the Aβ-negative from Aβ-positive cases; area under the ROC curve (AUROC) were .62 in OC, .77 in MCI, and .97 in ADdem. The visual score was not related to Aβ status in the non-AD clinical group (AUROC = .47, p = .79). Group comparisons were comparable when looking at each reader separately or considering the global cortical SUVR (Figure S3 in supporting information).

ROC analyses were used to determine the ability of the global visual score to distinguish Aβ-positive patients with MCI and AD dementia from all other cases (Figure 3C). The average visual score (AUROC = .92 [.88 to .94]; optimal threshold value ≥7, resulting in 78% sensitivity and 96% specificity) performed significantly better (P = .003) than global cortical SUVR (AUROC = .83 [.78 to .88]), but not different (P = .39) from the temporal meta-ROI (AUROC = .90 [.85, .93]).

3.3 | FTP patterns: reliability

When attributing one of the four visual patterns to the 274 scans, the two readers agreed in 66% of cases (compared to a chance level of 25% based on a four-pattern classification), and the inter-rater reliability was moderate (κ = .53 [.45 to .61]; Figure 4A and Figure S4 in supporting information). Most disagreement cases (26% of all scans) were "minor." "Major" disagreements (ie, between AD-like patterns and either negative or non-AD patterns) happened in 22 (8%) of all scans (Figure S5 in supporting information). Out of these 18 discrepant cases, 7 were OC (6 Aβ-negative), 10 were MCI (9 Aβ-negative) and 1 was an Aβ-negative case with a non-AD diagnosis; 16/18 were ADNI cases.

When separating the AD-like pattern versus any of the other three, the two readers agreed on 237/274 cases (86% agreement, κ = .71 [.62 to .79]). Other patterns had low inter-reader agreement (κ values between .39 and .49, Figure S4). Intra-rater reliability was good for the

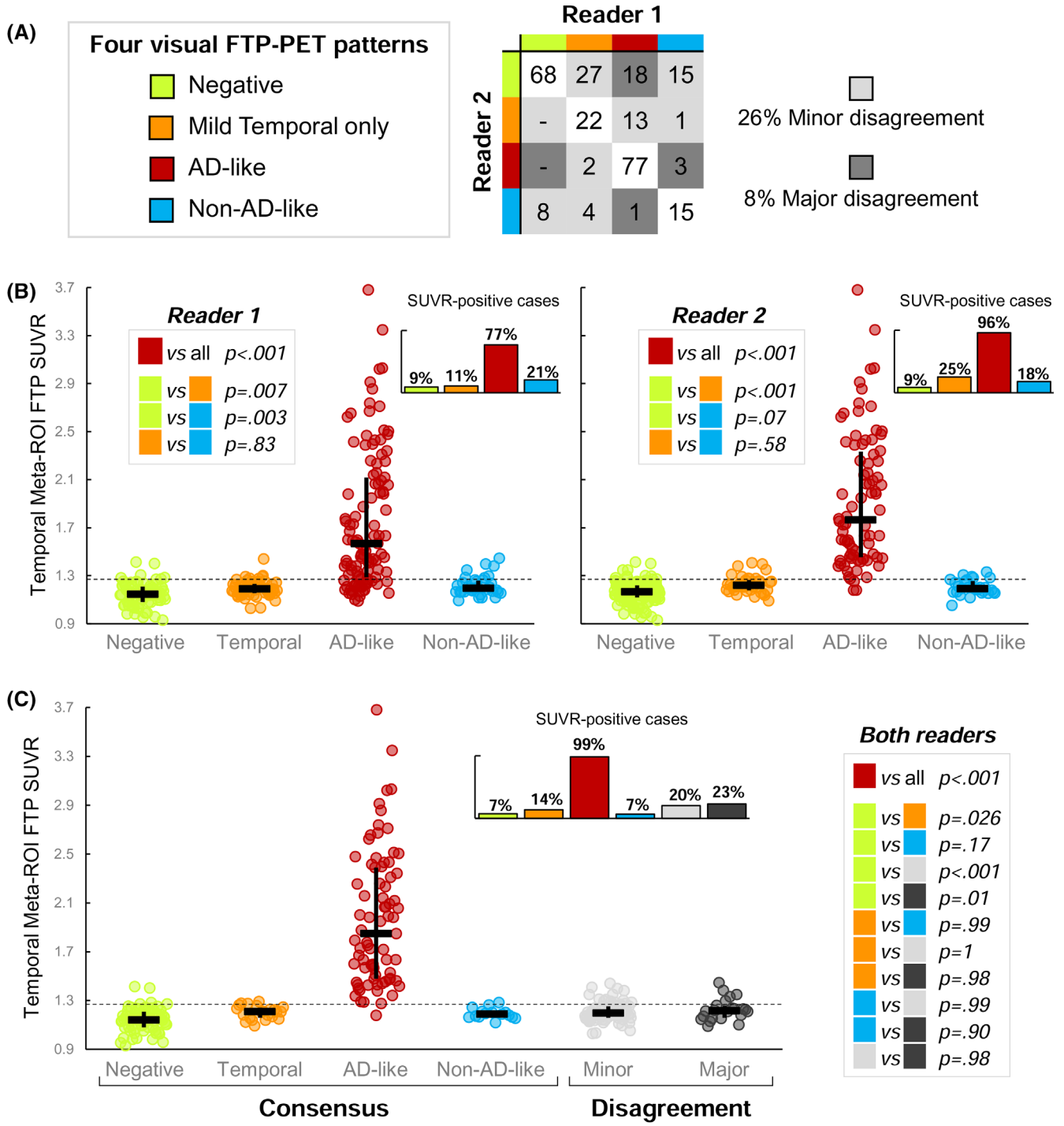

FIGURE 4 Visual flortaucipir patterns: inter-reader agreement and association with temporal meta-region of interest (ROI) standardized uptake value ratio (SUVR). A, Inter-reader agreement based on the 274 cases read by both readers (see Results section and Figure S4 in supporting information for statistics or intra-rater agreement). Numbers in the table indicate raw numbers of cases for each combination of patterns, not percentages. B, Association between temporal meta-ROI FTP-SUVR and visual patterns defined by each reader in the 274 cases. The dotted line represents the independently defined 1.27 threshold; small bar graph inserts indicate the proportion of case above the 1.27 threshold within each visual pattern group. Black bars show median and interquartile range. *P* values correspond to post hoc tests following significant Kruskal Wallis test (see Result section). C, Similar to panel (B), but distinguishing cases for which the two readers assigned similar or different visual patterns. The right panel shows the discriminative characteristics of the visual AD-like pattern to separate the two groups.

definition of the four patterns ($\kappa_{reader1} = .76$ and $\kappa_{reader2} = .79$) and for the distinction of the AD-like pattern versus any other ($\kappa_{reader1} = .73$, $\kappa_{reader2} = .92$; Figure S4).

3.4 | FTP patterns: relationship to visual scores and SUVR quantification

Negative patterns had very minimal global visual scores, showing a floor effect (>95% of cases with a score of 0). In contrast, AD-like patterns had median visual scores of 12 (reader 1) or 13 (reader 2), and reached a ceiling effect >40% cases being assigned the maximal score (Figure S6 in supporting information). The other patterns were associated with mildly elevated visual scores with median values around 2 to 4.

Figure 4B shows that FTP temporal meta-ROI SUVR strongly varied across visually determined patterns (Kruskal-Wallis test: $P < .001$, $\varepsilon^2 = .49$ for reader 1; $P < .001$, $\varepsilon^2 = .62$ for reader 2). For both readers, the AD-like pattern was associated with higher SUVR values than all other patterns (all Ps <.001). Most patients classified as AD-like had temporal SUVR values > 1.27 (77% for reader 1, 96% for reader 2). The mild temporal and the non-AD-like patterns showed significantly increased temporal meta-ROI SUVR values compared to the negative pattern at the group level, but most cases remained <1.27 (Figure 4B). When readers disagreed, reader 2 was usually more conservative than reader 1 (Figure 4A), and 20% to 23% of these scans had temporal meta-ROI SUVR >1.27 threshold (Figure 4C).

3.5 | FTP patterns across diagnoses and Aβ status

Both readers assigned the AD-like pattern to the vast majority of Aβ-positive ADdem, around half Aβ-positive MCI, and some Aβ-positive OC (reader 1: 12/31, reader 2: 8/31; Figure 5A). Reader 1 also classified 24 Aβ-negative participants (10/72 controls, 11/28 MCI, 1/3 ADdem, and 2/23 non-AD) as AD-like. The mild temporal binding visual pattern was found across clinical and Aβ subgroups. The non-AD-like FTP pattern was assigned to a large proportion of patients with a non-AD diagnosis (11/30 for reader 1, 16/30 for reader 2) and some cases from other subgroups. Similarly, tau-positive cases defined by temporal meta-ROI SUVR > 1.27, were found in the majority of Aβ-positive patients with MCI and ADdem, but also in other subgroups (Figure 5B).

The AD-like pattern was far more frequent in Aβ-positive patients with MCI or ADdem (reader 1: 73/90, reader 2: 70/90) than in other participants (reader 1: 36/184, reader 2: 12/184). Very few Aβ-positive MCI/ADdem patients were attributed a negative FTP pattern (reader 1: 3/90, reader 2: 7/90). The AD-like pattern had good sensitivity (78% to 81%) and good to excellent specificity (80% to 93%). The AD-like pattern had discrimination performances comparable to tau-positivity based on the temporal meta-ROI (82% sensitive, 84% specific). When combining patterns from both readers, the sensitivity of the AD-like pattern (assigned by both readers) was 76%, but the specificity reached 95% (Figure S7 in supporting information).

4 | DISCUSSION

We developed and evaluated a visual rating scheme for the qualitative interpretation of FTP tau PET scans. We tested this visual approach in a large (n = 274) multi-center sample derived from two independent cohorts with the intent to encompass the heterogeneity of a clinical population, including various clinical diagnoses, and using PET data acquired from multiple sites. Results indicate that the interpretation of FTP-PET using our visual approach strongly correlates with SUVR quantification and is associated with both clinical diagnosis and Aβ status.

The two visual indices we developed (a global score and an AD-like visual pattern) allowed the differentiation of Aβ-positive patients with MCI or AD dementia from other participants with ≈78% to 81% sensitivity and ≈80% to 96% specificity, similar to the SUVR quantification of temporal signal in the same patients (82% sensitivity, 84% specificity, Figure 4). Regardless of the visual or SUVR-based definition of tau-positivity, "false negative" cases were more likely to be patients with MCI rather than dementia, suggesting that all the proposed approaches might be missing lower tau levels. Alternatively, it is possible that these FTP-negative Aβ-positive patients did not harbor any tau pathology, and that their cognitive deficits might be due to another, non-AD etiology. Within the recently proposed NIA-AA research framework[37] these cases would correspond to "Alzheimer's pathologic change [rather than full AD, ie, Aβ + tau] with concomitant non-AD changes." Inversely, a visual score >7 or an AD-like visual pattern was frequent in Aβ-positive OC, suggesting that the visual indices might capture tau pathology at the preclinical stage. Additional "false positives" visual FTP-PET were found in Aβ-negative subjects (Figure 4A and Figure S4). The absence of autopsy data does not make it possible to clarify whether these are true false positive (ie, positive FTP-PET without underlying tau pathology, for instance due to off-target binding related to non-tau related pathology),[38] or represent neurofibrillary pathology without Aβ such as primary age-related tauopathy (PART).[39,40]

In parallel to our effort, Avid Radiopharmaceuticals developed an independent visual read method consisting of separating FTP-PET patterns consistent with AD (with an additional distinction between moderate and advanced patterns) from negative tau patterns.[19] Although no formal head-to-head comparison was conducted between the two protocols, our approach and Avid's largely overlap, and equivalences can be drawn. Avid's "negative" patterns encompasses our own negative pattern (pattern I, no activity beyond off-target binding), scans with isolated mesial temporal signal (our pattern II), or increased neocortical activity isolated to the anterolateral temporal, and/or frontal regions (which would likely be classified as our pattern IV). The identification of Avid's "AD tau pattern" relied on the presence of signal in the postero-lateral temporal or occipital regions, and additional parietal/precuneus or frontal binding to be considered "advanced" AD tau; these scans would be classified as "AD-like" (pattern III) in our visual scheme. The Avid protocol was used in an end-of-life study including 64 terminally ill participants (50 cognitively impaired, 14 cognitively unimpaired) to test the association with *post mortem* findings.

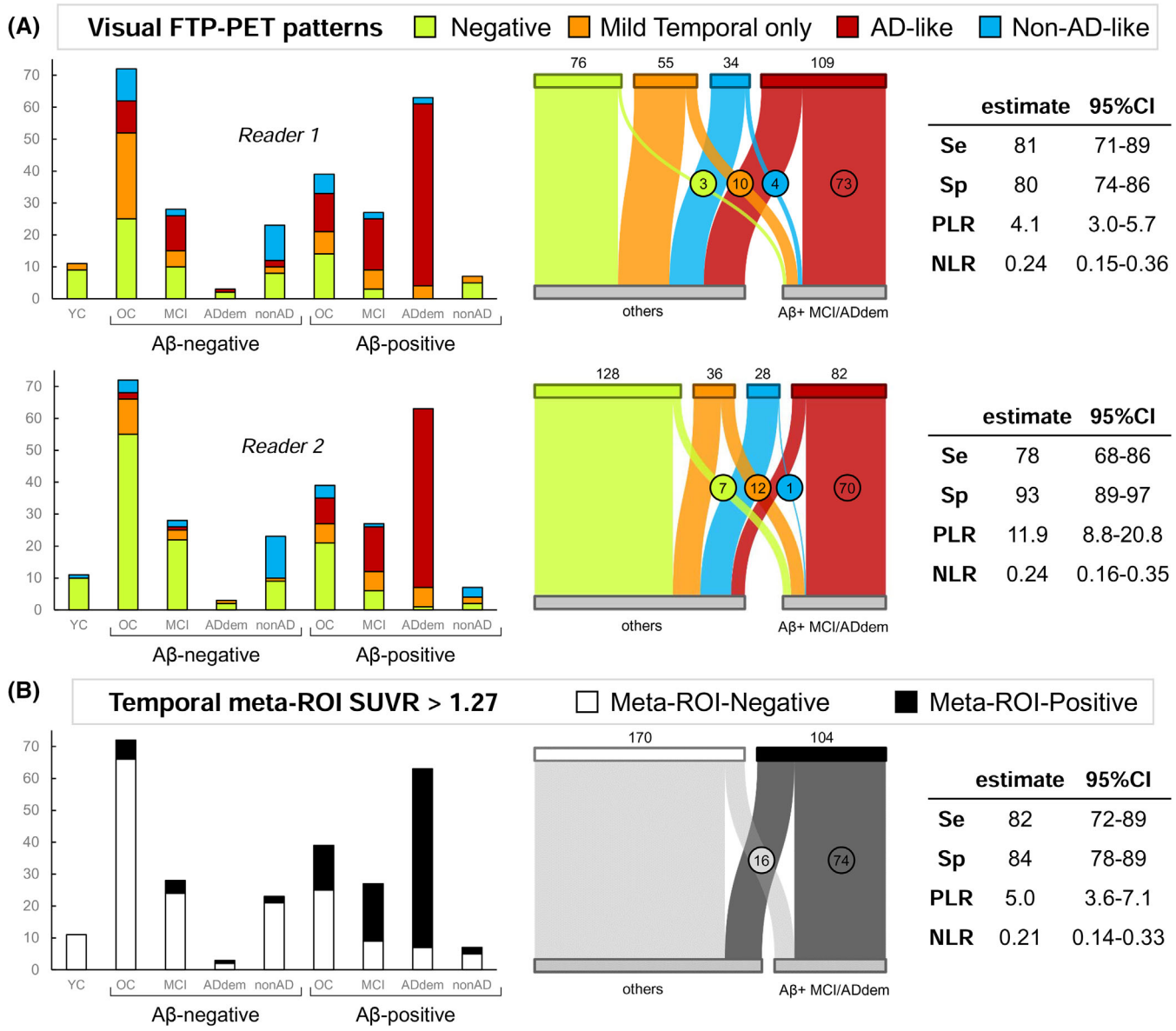

FIGURE 5 Visual flortaucipir patterns and temporal meta- region of interest (ROI) standardized uptake value ratio (SUVR)-based positivity: association with clinical diagnosis and amyloid beta (Aβ) status. A, FTP visual patterns assigned by each reader (top: reader 1, bottom: reader 2; see Figure S7 in supporting information for the combination of both readers). Left panel shows the distribution of visual patterns (y-axis) in each clinical/Aβ subgroup (x-axis). Middle panel illustrates the distribution of visual patterns (specific n indicated on top), and in Aβ-positive MCI/ADdem (circled numbers, n = 90 total), versus all other participants (n = 184). Right panel shows the diagnostic properties of the AD-like pattern to distinguish Aβ-positive MCI/ADdem versus all other participants. (B) Distribution of temporal SUVR-based tau-positive cases in each clinical/Aβ subgroup (left) or in Aβ-positive MCI/ADdem versus all other participants (middle). Right panel shows the diagnostic properties of the meta-ROI-based FTP positivity to distinguish Aβ-positive MCI/ADdem versus all other participants. YC, young controls; OC, older controls; MCI, patients with a clinical diagnosis of mild cognitive impairment; ADdem, patients with a clinical diagnosis of Alzheimer's disease dementia; non-AD, patients with a clinical diagnosis of non-AD neurodegenerative syndrome. Clinical diagnoses were independent from Aβ status. Se, sensitivity; Sp, specificity; PLR, positive likelihood ratio; NLR, negative likelihood ratio

An AD-tau pattern was able to detect patients with Braak stages V-VI (sensitivity: 92.3% to 100% based on five independent readers; specificity: 52% to 92%) or with high AD neuropathologic changes (ie, Braak V/VI with high amyloid burden; sensitivity: 94.7% to 100%; specificity: 50% to 92.3%). In patients with lower stages of tau pathology, most scans were read as negative (75% for Braak IV, 80% for Braak III, and 83% for Braak II), and were all negative based on image quantification.

In spite of differences in the visual approach and study design, our data support the Avid results as both studies show that FTP-PET visual reads are feasible and can identify advanced cases of clinically diagnosed AD or AD pathology with high accuracy, supporting its translation to clinical settings.

Both the global visual score and the identification of an AD-like pattern showed satisfactory intra- and inter-reader agreement ($\kappa s \geq .71$),

underlying the reliability of the main indices of interest derived from our visual rating scheme. However, the inter-reader agreement on the four-pattern distinction was only moderate (κ = .53), and the specific identification of the other three patterns were suboptimal (κs <.5, Figure S4). The difficulty in identifying these patterns can be attributed to the lower amount of tau-PET signal associated with them and to some choices we made in the development of our visual scheme. Indeed, our approach focused on identifying a clear AD pattern based on a limited amount of data and data pre-processing so that it could be widely used in clinical settings. Thus, visual reads were based on non-intensity normalized images to make this method accessible without a dedicated neuro-software. Image contrast had to be adjusted by each reader, resulting in intrinsic variability in the reading process. Alternative approaches, including reading an SUVR image or access to more advanced quantification methods might help improve pattern identification, similar to recent propositions related to amyloid-PET.[41–43] Morever, FTP scans were read without any anatomical (computed tomography or MRI) imaging while it could help PET interpretation by highlighting macroscopic abnormalities (eg, atrophy, presence of vascular anomalies or meningiomas[44]) and better distinguishing cortical from white matter signal. Anatomical information could be particularly helpful to identify the "mild temporal binding" pattern due to the multiple sources of off-target binding in areas surrounding the areas of interest (eg, choroid plexus, extra-brain binding medial to the entorhinal/parahippocampal areas).

The main challenge to an FTP-PET visual approach relates to the presence of off-target binding. Contrary to amyloid imaging, in which white matter predominant off-target binding is a constant feature across Aβ-radiotracers and is key to the interpretation of PET scan,[45–47] FTP-PET off-target signal is highly variable across individuals both in terms of severity and location, therefore hampering FTP interpretability.[48] Various factors are suspected to cause FTP off-target signal: neuromelanin, brain hemorrhagic lesions, as well as the enzymes monoamine oxidase (MAO)-A and MAO-B, widely distributed throughout the brain in both neurons and glia.[8,48,49] Sufficient knowledge of FTP off-target binding is fundamental to the accurate interpretation of the PET scan.

In conclusion, our study shows that the proposed visual ratings of FTP tau PET are strongly associated with FTP global quantification, clinical diagnosis, and Aβ status across two cohorts with distinct characteristics. Inter- and intra-rater reliability for our main indices are strong, suggesting that the proposed visual approach is reproducible and can therefore represent a promising alternative to quantitative tau-PET measurements in clinical settings. Future investigations including an autopsy-based gold standard are needed to evaluate the exact potential and limitations of tau-PET and the proposed visual read approach.

FUNDING INFORMATION

Data collection and sharing for this project was funded by the Alzheimer's Disease Neuroimaging Initiative (ADNI; National Institutes of Health Grant U01 AG024904) and DOD ADNI (Department of Defense award number W81XWH-12-2-0012). ADNI is funded by the National Institute on Aging, the National Institute of Biomedical Imaging and Bioengineering, and through generous contributions from the following: AbbVie; Alzheimer's Association; Alzheimer's Drug Discovery Foundation; Araclon Biotech; BioClinica, Inc.; Biogen; Bristol-Myers Squibb Company; CereSpir, Inc.; Cogstate; Eisai Inc.; Elan Pharmaceuticals, Inc.; Eli Lilly and Company; EuroImmun; F. Hoffmann-La Roche Ltd and its affiliated company Genentech, Inc.; Fujirebio; GE Healthcare; IXICO Ltd.; Janssen Alzheimer Immunotherapy Research & Development, LLC; Johnson & Johnson Pharmaceutical Research & Development LLC; Lumosity; Lundbeck; Merck & Co., Inc.; Meso Scale Diagnostics, LLC; NeuroRx Research; Neurotrack Technologies; Novartis Pharmaceuticals Corporation; Pfizer Inc.; Piramal Imaging; Servier; Takeda Pharmaceutical Company; and Transition Therapeutics. The Canadian Institutes of Health Research is providing funds to support ADNI clinical sites in Canada. Private sector contributions are facilitated by the Foundation for the National Institutes of Health (www.fnih.org). The grantee organization is the Northern California Institute for Research and Education, and the study is coordinated by the Alzheimer's Therapeutic Research Institute at the University of Southern California. ADNI data are disseminated by the Laboratory for Neuro Imaging at the University of Southern California. The BACS/UCSF cohorts receive funding from National Institute on Aging grants (R01-AG045611.; R01-AG034570; R01-AG062542; P50-AG023501; P01-AG19724 to) and the Rainwater Charitable Foundation. Renaud La Joie n funded by the Alzheimer's Association (AARF:16-443577) and the National Institute of Aging (K99AG065501). Avid Radiopharmaceuticals enabled use of the [18F]Flortaucipir tracer by providing precursor, but did not provide direct funding and was not involved in data analysis or interpretation.

ETHICAL APPROVAL

The Institutional Review Boards of all participating institutions approved the study and informed consent was obtained from all participants or authorized representatives. The study procedures were in accordance with the institutional ethical standards and with the 1964 Helsinki declaration and its later amendments.

CONFLICTS OF INTEREST

Suzanne L. Baker serves as a consultant for Genentech. No other potential conflicts of interest relevant to this article exist. Gil D. Rabinovici has research support from Avid Radiopharmaceuticals, GE Healthcare, Eli Lilly, and Life Molecular Imaging; has served as a consultant for Axon Neurosciences, GE Healthcare, Eisai, and Merck; and is an Associate Editor for *JAMA Neurology*. No other potential conflicts of interest relevant to this article exist. William J. Jagust serves as a consultant to Bioclinica, Genentech, CuraSen, Biogen, and Grifols and owns equity in OptoCeutics. No other potential conflicts of interest relevant to this article exist. Susan M. Landau has served as a consultant for NeuroVision and Cortexyme. No other potential conflicts of interest relevant to this article exist. No potential conflicts of interest relevant to this article exist for all other authors.

ORCID

Ida Sonni https://orcid.org/0000-0002-8802-7704
Renaud La Joie https://orcid.org/0000-0003-2581-8100

REFERENCES

1. Frisoni GB, Boccardi M, Barkhof F, et al. Strategic roadmap for an early diagnosis of Alzheimer's disease based on biomarkers. *Lancet Neurol*. 2017;16:661-676.
2. McKhann GM, Knopman DS, Chertkow H, et al. The diagnosis of dementia due to Alzheimer's disease: recommendations from the National Institute on Aging-Alzheimer's Association workgroups on diagnostic guidelines for Alzheimer's disease. *Alzheimer's Dement*. 2011;7:263-269.
3. Klunk WE, Engler H, Nordberg A, et al. Imaging brain amyloid in Alzheimer's disease with Pittsburgh Compound-B. *Ann Neurol*. 2004;55:306-319.
4. Barthel H, Gertz HJ, Dresel S, et al. Cerebral amyloid-beta PET with florbetaben (18F) in patients with Alzheimer's disease and healthy controls: a multicentre phase 2 diagnostic study. *Lancet Neurol*. 2011;10:424-435.
5. Clark CM, Schneider JA, Bedell BJ, et al. Use of florbetapir-PET for imaging beta-amyloid pathology. *JAMA*. 2011;305:275-283.
6. Vandenberghe R, Van Laere K, Ivanoiu A, et al. 18F-flutemetamol amyloid imaging in Alzheimer disease and mild cognitive impairment: a phase 2 trial. *Ann Neurol*. 2010;68:319-329.
7. Clark CM, Pontecorvo MJ, Beach TG, et al. Cerebral PET with florbetapir compared with neuropathology at autopsy for detection of neuritic amyloid-beta plaques: a prospective cohort study. *Lancet Neurol*. 2012;11:669-678.
8. Leuzy A, Chiotis K, Lemoine L, et al. Tau PET imaging in neurodegenerative tauopathies-still a challenge. *Mol Psychiatry*. 2019;24(8):1112-1134.
9. Lowe VJ, Curran G, Fang P, et al. An autoradiographic evaluation of AV-1451 Tau PET in dementia. *Acta Neuropathol Commun*. 2016;4:58.
10. Marquie M, Normandin MD, Vanderburg CR, et al. Validating novel tau positron emission tomography tracer [F-18]-AV-1451 (T807) on postmortem brain tissue. *Ann Neurol*. 2015;78:787-800.
11. Xia CF, Arteaga J, Chen G, et al. [(18)F]T807, a novel tau positron emission tomography imaging agent for Alzheimer's disease. *Alzheimer's Dement*. 2013;9:666-676.
12. Marquie M, Siao T, Chong M, et al. [F-18]-AV-1451 binding correlates with postmortem neurofibrillary tangle Braak staging. *Acta Neuropathol*. 2017;134:619-628.
13. Bejanin A, Schonhaut DR, La Joie R, et al. Tau pathology and neurodegeneration contribute to cognitive impairment in Alzheimer's disease. *Brain*. 2017;140:3286-300.
14. La Joie R, Bejanin A, Fagan AM, et al. Associations between [(18)F]AV1451 tau PET and CSF measures of tau pathology in a clinical sample. *Neurology*. 2018;90:e282-e290.
15. Meyer PF, Binette AP, Gonneaud J, Breitner JCS, Villeneuve S. Characterization of Alzheimer disease biomarker discrepancies using cerebrospinal fluid phosphorylated tau and AV1451 positron emission tomography. *JAMA Neurol*. 2020;77(4):508-516.
16. Thijssen EH, La Joie R, Wolf A, et al. Diagnostic value of plasma phosphorylated tau181 in Alzheimer's disease and frontotemporal lobar degeneration. *Nature Med*. 2020;26:387-397.
17. Smith R, Wibom M, Pawlik D, Englund E, Hansson O. Correlation of In Vivo [18F]Flortaucipir With Postmortem Alzheimer Disease Tau Pathology. *JAMA Neurol*. 2019;76:310-317.
18. Fleisher AS, Pontecorvo MJ, Devous MD Sr., et al. Positron Emission Tomography Imaging With [18F]flortaucipir and Postmortem Assessment of Alzheimer Disease Neuropathologic Changes. *JAMA Neurol*. 2020;77 (7):829–839.
19. Hanseeuw BJ, Betensky RA, Schultz AP, et al. Fluorodeoxyglucose metabolism associated with tau-amyloid interaction predicts memory decline. *Ann Neurol*. 2017;81:583-596.
20. Maass A, Landau S, Baker SL, et al. Comparison of multiple tau-PET measures as biomarkers in aging and Alzheimer's disease. *NeuroImage*. 2017;157:448-463.
21. La Joie R, Visani AV, Baker SL, et al. Prospective longitudinal atrophy in Alzheimer's disease correlates with the intensity and topography of baseline tau-PET. *Sci Transl Med*. 2020;12:eaau5732.
22. Ossenkoppele R, Rabinovici GD, Smith R, et al. Discriminative Accuracy of [18F]flortaucipir Positron Emission Tomography for Alzheimer Disease vs Other Neurodegenerative Disorders. *JAMA*. 2018;320:1151-1162.
23. Scholl M, Lockhart SN, Schonhaut DR, et al. PET imaging of tau deposition in the aging human brain. *Neuron*. 2016;89:971-982.
24. Baker SL, Maass A, Jagust WJ. Considerations and code for partial volume correcting [(18)F]-AV-1451 tau PET data. *Data Brief*. 2017;15:648-657.
25. Maass A, Berron D, Harrison TM. Alzheimer's pathology targets distinct memory networks in the ageing brain. *Brain*. 2019;142:2492-2509.
26. Petersen RC, Aisen PS, Beckett LA, et al. Alzheimer's Disease Neuroimaging Initiative (ADNI): clinical characterization. *Neurology*. 2010;74:201-209.
27. Landau SM, Breault C, Joshi AD, et al. Amyloid-beta imaging with Pittsburgh compound B and florbetapir: comparing radiotracers and quantification methods. *J Nucl Med*. 2013;54:70-77.
28. Landau SM, Marks SM, Mormino EC, et al. Association of lifetime cognitive engagement and low beta-amyloid deposition. *Arch Neurol*. 2012;69:623-629.
29. Mormino EC, Brandel MG, Madison CM, et al. Not quite PIB-positive, not quite PIB-negative: slight PIB elevations in elderly normal control subjects are biologically relevant. *NeuroImage*. 2012;59:1152-1160.
30. Ossenkoppele R, Cohn-Sheehy BI, La Joie R, et al. Atrophy patterns in early clinical stages across distinct phenotypes of Alzheimer's disease. *Hum Brain Mapp*. 2015;36:4421-4437.
31. Villeneuve S, Rabinovici GD, Cohn-Sheehy BI, et al. Existing Pittsburgh Compound-B positron emission tomography thresholds are too high: statistical and pathological evaluation. *Brain*. 2015;138:2020-2033.
32. Braak H, Alafuzoff I, Arzberger T, Kretzschmar H, Del Tredici K. Staging of Alzheimer disease-associated neurofibrillary pathology using paraffin sections and immunocytochemistry. *Acta Neuropathol*. 2006;112:389-404.
33. Braak H, Braak E. Neuropathological stageing of Alzheimer-related changes. *Acta Neuropathol*. 1991;82:239-259.
34. Schwarz AJ, Yu P, Miller BB, et al. Regional profiles of the candidate tau PET ligand 18F-AV-1451 recapitulate key features of Braak histopathological stages. *Brain*. 2016;139:1539-1550.
35. Cho H, Choi JY, Hwang MS, et al. In vivo cortical spreading pattern of tau and amyloid in the Alzheimer disease spectrum. *Ann Neurol*. 2016;80:247-258.
36. Tsai RM, Bejanin A, Lesman-Segev O, et al. (18)F-flortaucipir (AV-1451) tau PET in frontotemporal dementia syndromes. *Alzheimers Res Ther*. 2019;11:13.
37. Jack CR, Jr., Bennett DA, Blennow K, et al. NIA-AA Research Framework: Toward a biological definition of Alzheimer's disease. *Alzheimer's Dement*. 2018;14:535-562.
38. Smith R, Santillo AF, Waldo ML, et al. (18)F-Flortaucipir in TDP-43 associated frontotemporal dementia. *Sci Rep*. 2019;9:6082.
39. Crary JF, Trojanowski JQ, Schneider JA, et al. Primary age-related tauopathy (PART): a common pathology associated with human aging. *Acta Neuropathol*. 2014;128:755-766.
40. Kim D, Kim HS, Choi SM, et al. Primary Age-Related Tauopathy: an elderly brain pathology frequently encountered during autopsy. *J Pathol Transl Med*. 2019;53:159-163.

41. Belohlavek O, Jaruskova M, Skopalova M, Szarazova G, Simonova K. Improved beta-amyloid PET reproducibility using two-phase acquisition and grey matter delineation. *Eur J Nuclr Med Mol Imaging*. 2019;46:297-303.
42. Chincarini A, Peira E, Morbelli S, et al. Semi-quantification and grading of amyloid PET: A project of the European Alzheimer's Disease Consortium (EADC). *NeuroImage Clin*. 2019;23:101846.
43. Harn NR, Hunt SL, Hill J, Vidoni E, Perry M, Burns JM. Augmenting amyloid pet interpretations with quantitative information improves consistency of early amyloid detection. *Clin Nucl Med*. 2017;42:577-581.
44. Lockhart SN, Ayakta N, Winer JR, La Joie R, Rabinovici GD, Jagust WJ. Elevated (18)F-AV-1451 PET tracer uptake detected in incidental imaging findings. *Neurology*. 2017;88:1095-1097.
45. Hosokawa C, Ishii K, Hyodo T, et al. Investigation of (11)C-PiB equivocal PET findings. *Ann Nucl Med*. 2015;29:164-169.
46. Lockhart A, Lamb JR, Osredkar T, et al. PIB is a non-specific imaging marker of amyloid-beta (Abeta) peptide-related cerebral amyloidosis. *Brain*. 2007;130:2607-2615.
47. Matsubara K, Ibaraki M, Shimada H, et al. Impact of spillover from white matter by partial volume effect on quantification of amyloid deposition with [(11)C]PiB PET. *NeuroImage*. 2016;143:316-324.
48. Baker SL, Harrison TM, Maass A, La Joie R, Jagust WJ. Effect of off-target binding on (18)F-Flortaucipir variability in healthy controls across the life span. *J Nucl Med*. 2019;60:1444-1451.
49. Barrio JR. The irony of PET tau probe specificity. *J Nucl Med*. 2018;59:115-116.

SUPPORTING INFORMATION

Additional supporting information may be found online in the Supporting Information section at the end of the article.

How to cite this article: Sonni I, Lesman Segev OH, Baker SL, et al. Evaluation of a visual interpretation method for tau-PET with ^{18}F-flortaucipir. *Alzheimer's Dement*. 2020;12:e12133. https://doi.org/10.1002/dad2.12133